

We are IntechOpen, the world's leading publisher of Open Access books Built by scientists, for scientists

6,900

Open access books available

185,000

International authors and editors

200M

Downloads

Our authors are among the

154

Countries delivered to

TOP 1%

most cited scientists

12.2%

Contributors from top 500 universities



WEB OF SCIENCE™

Selection of our books indexed in the Book Citation Index
in Web of Science™ Core Collection (BKCI)

Interested in publishing with us?
Contact book.department@intechopen.com

Numbers displayed above are based on latest data collected.
For more information visit www.intechopen.com



Network Methods for Analysis and Design of Resonant Wireless Power Transfer Systems

Marco Dionigi¹, Alessandra Costanzo² and Mauro Mongiardo¹

¹University of Perugia

²University of Bologna

Italy

1. Introduction

1.1 A taxonomy of electromagnetic energy transfer

Efficient energy transfer is nowadays becoming an essential topic: it allows to save economical resources, to improve the quality of life, to reduce pollution, to name just a few issues. In particular, energy transfer is often realized by using electromagnetic power which can either be transmitted along a guiding medium (transmission lines), or without a supporting medium. Waveguiding structures can possess a discrete spectrum, as e.g. metallic waveguides or, in the instance of waveguides with unbounded cross section, a continuous spectrum (or both). These cases are well known and a considerable literature exists for their analysis and design, see e.g. Collin (1960), Rozzi (1997). Unfortunately, guided waves require the presence of a medium to support wave propagation; in addition, energy decays along the transmission lines in an exponential manner.

A different mechanism for transmitting electromagnetic energy is that of radiation; note that also in this case a generalized network representation is feasible in terms of spherical modes, as described in Felsen (2009), Mongiardo et al. (2009). Naturally, at microwave frequencies, the antennas become more directive as the frequency is increased (and, therefore, the dimensions of the antenna with respect to the wavelength are also increased). On the other hand, propagation at very high frequencies may pose problems due to the atmospheric attenuation, availability of hardware components, etc. In addition, radiated energy is spread over radiation angles and its attenuation goes with an inverse quadratic law with respect to distance, even in the case of vacuum.

Another possibility for transmitting electromagnetic energy is by using the reactive fields present nearby open resonators, as recently suggested in Kurs et al. (2007) and Karalis et al. (2008). In fact, two open structures operating at the same resonant frequency may exchange energy. It suffices a very low coupling for the energy transfer to take place and, in presence of "perfects" infinite Q resonators, even a very weak coupling will provide the possibility of transferring energy to the load (which is the only places where energy can be dissipated since, by definition, the resonators are lossless). In practice, by placing many resonators physically separated by one another, it is possible to realize a wireless power transfer based on the near field characteristics and avoiding both radiation and the presence of a conducting media. It is clear that the type of energy transfer that can be achieved depends on the coupling and on the

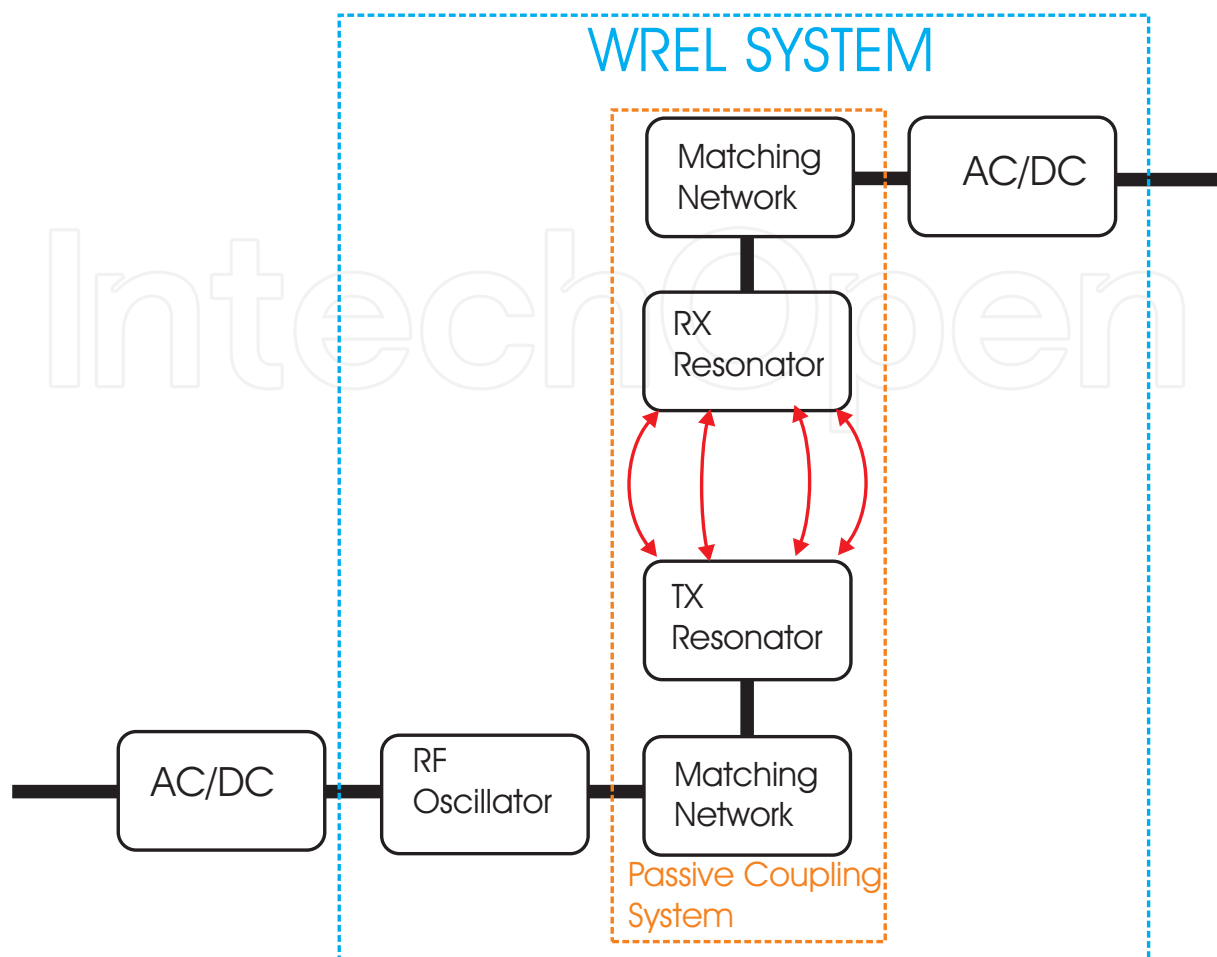


Fig. 1. Sketch of a typical system for resonant Wireless Power Transfer (WPT). Apart for AC/DC converters we note the presence of a RF oscillator and a transmitting (TX) resonator, a receiving (RX) resonator and matching networks to couple the energy from the RF oscillator to the TX resonator and from the RX resonator to the AC/DC converter. Note that the part between the output of the RF oscillator and the input of the AC/DC converter, denoted as passive coupling system in the figure, is a two port network containing only linear, passive, components.

quality factor of the resonators. As we will see in this chapter, this problem can be formalized in an accurate and rigorous manner by using network theory. By using the latter, it is possible to find out to what extent this resonant reactive field coupling can be employed in various applications. Note that the resonant coupling which we are referring to is very different from inductive coupling, which is suitable only for very short range; a nice comparison between these two types of wireless energy transfer has been published in Cannon et al. (2009). Also observe that we look for magnetic field coupling which has the advantage, with respect to electric field coupling, to be rather insensitive to the presence of different dielectrics. It is also worthwhile to consider that, in order to avoid radiation, it is preferable that the electric field storage takes place in a confined region of space, which may be physically realized either by a lumped capacitance or by other suitable structures.

1.1.1 A word about nomenclature

The energy exchange which we are interested to in this chapter is the one that occurs when two, or more, structure resonates at the same frequency and exchange their energy. This type of phenomenology has been referred to in the literature with several different names: Wireless Resonant Energy Links (WREL), Wireless Power Transfer (WPT), WITRICITY (Wireless electRICITY), Wireless Energy Transfer (WET), etc. Each different name possesses its own advantages and disadvantages; it is only necessary to keep in mind that, in this work, we are referring to *resonant* structures and we are not referring to antennas (which mainly serve to produce a radiated field). Note, in addition, that a radiated field is, in this type of application, particularly undesirable since it poses increased problems of electromagnetic compatibility.

1.2 Description of a typical system for medium–range resonant power transfer

In Fig.1 we have reported the sketch of a typical system for WPT. Apart from AC/DC converters we note the presence of a RF oscillator and a transmitting (TX) resonator, a receiving (RX) resonator and matching networks to couple the energy from the RF oscillator to the TX resonator and from the RX resonator to the AC/DC converter. Note that the subnetwork between the output of the RF oscillator and the input of the AC/DC converter is a linear system; this part can be described as a two port network containing only linear, passive, components. An example of a practical implementation of this part is reported in Fig.2. In the next section we will show why this type of structure is advantageous for realizing efficient WPT.

1.3 Plan of the chapter

In sec. 2 we introduce a simple network that, nonetheless, allows us to understand resonant WPT. In that section we will find why it is convenient to introduce matching networks for improving the efficiency of wireless energy transfer. In addition, the complete network (including the matching sections), which describe the linear, passive, part of a WPT system, permits derivation of a relationship between the radio frequency (RF) efficiency and the parameters (quality factor Q , coupling) of the resonators. In this way, theoretical limits can be established and the range for WPT and its efficiency are related to the resonators' parametrization (Q and coupling). A couple of examples of implementations are also illustrated in order to verify what is experimentally feasible for a WPT system operating at a fixed distance.

The next section, sec. 3, deals with the analysis method for a more general case: we consider a methodology which allows the analysis when multiple TX and RX resonators are present. In particular, we note that, by adding further resonators, it is possible to extend the range for WPT. In that section also an approach useful for analyzing this type of network with a common circuit simulator (SPICE) is illustrated.

A crucial block of an inductive power link system is the external power driving unit. The design of this part of the system is considered in sec. 4; in this section we introduce a type of oscillator suitable for resonant WPT. When considering inductive links over variable distances, we observe that the resonant frequency of the system shifts. The proposed power driving unit automatically adjust itself, thus providing a convenient implementation. An example, along with its experimental verification, is also presented.

The quality factor of the resonators is also one of the key elements in the design of resonant WPT system; sec. 5 describes how to measure the Q for a given resonator. Finally, conclusions are summarized in the last section.



Fig. 2. A structure showing the inductive coupling between the source (first loop on the left), the transmitting resonator (second coil from the left), receiving resonator (third coil from the left) and load (last loop on the right).

2. Network theory for medium-range power transfer

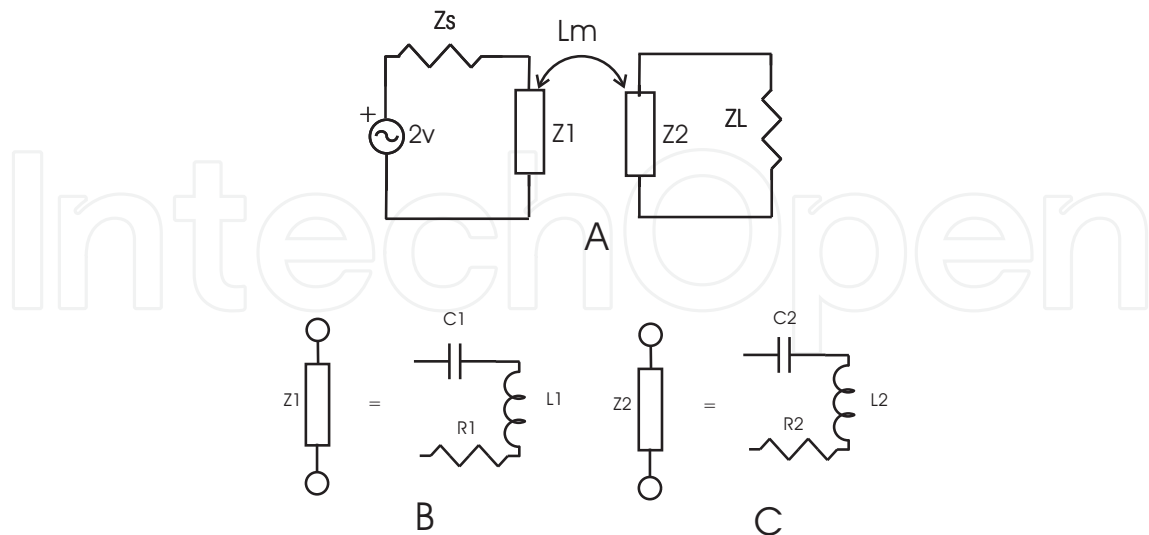


Fig. 3. A simple network for the study of wireless resonant energy links. The two resonators are described by Z_1 and Z_2 ; R_1 and R_2 take into account the losses in the resonators.

2.1 A simple network model for coupled resonators

A very simple network for understanding WREL is reported in Fig. 3, where Z_1 and Z_2 take into account the resonant element values, and Z_S , Z_L are the source and load impedances. By placing a generator of amplitude 2, the computation of S_{21} is quite straightforward. By denoting with I_1 the current flowing in the circuit on the left side and with I_2 the current flowing in the circuit on the right side, we may write Kirchhoff's voltage laws as:

$$2 = (Z_S + Z_1)I_1 - j\omega L_m I_2 \quad (1)$$

$$0 = (Z_L + Z_2)I_2 - j\omega L_m I_1 \quad (2)$$

After finding I_1 from I_2 by using the second eq., replacing it in the first eq. and solving, we obtain:

$$S_{21} = Z_L I_2 = \frac{2j\omega L_m Z_L}{(\omega L_m)^2 + (Z_S + Z_1)(Z_L + Z_2)} \quad (3)$$

It is convenient to define the efficiency of the linear, passive, two port network represented in Fig.1 as:

$$\eta = |S_{21}|^2 * 100 \quad (4)$$

By finding I_2 from I_1 , and by using the second eq. while denoting with Z_{in} the equivalent impedance in series with Z_S , we have that, for maximum power transfer, the following condition holds:

$$Z_S^* = Z_{in} = Z_1 + \frac{(\omega L_m)^2}{(Z_L + Z_2)} \quad (5)$$

2.1.1 Resonant frequencies

In order to realize resonant WPT, the two resonators must have an equal resonant frequency, i.e. $\omega_R = \frac{1}{\sqrt{L_1 C_1}} = \frac{1}{\sqrt{L_2 C_2}}$; as long as the resonator coupling is weak, the system has only this resonant frequency.

As the coupling increases we need to take into account also the effect of the other resonator. To compute the resonant frequencies, it is advantageous to derive an alternative network. With reference to Fig. 4 it is also possible to note that the circuit represented in Fig. 4A is equivalent to the circuit represented in Fig. 4B.

Let us consider the case of two identical resonators with $L_1 = L_2 = L$ and $C_1 = C_2 = C$. With reference to Fig. 4B, by defining $\omega_0 = \frac{1}{\sqrt{LC}}$ and $k = L_m/L$, and by considering even and odd excitations, corresponding to a magnetic (ω_m) and an electric resonance (ω_e) respectively, we get the following expressions for the resonant frequencies:

$$\omega_m = \frac{1}{\sqrt{(L + L_m)C}} = \frac{\omega_0}{\sqrt{1 + k}} \quad (6)$$

$$\omega_e = \frac{1}{\sqrt{(L - L_m)C}} = \frac{\omega_0}{\sqrt{1 - k}} \quad (7)$$

Note that for very small values of k , the resonant frequency is not affected by the presence of the other resonator. Naturally, as the resonators couple their fields, we note that two resonant frequencies appear; in addition, by changing the position of one resonator with respect to

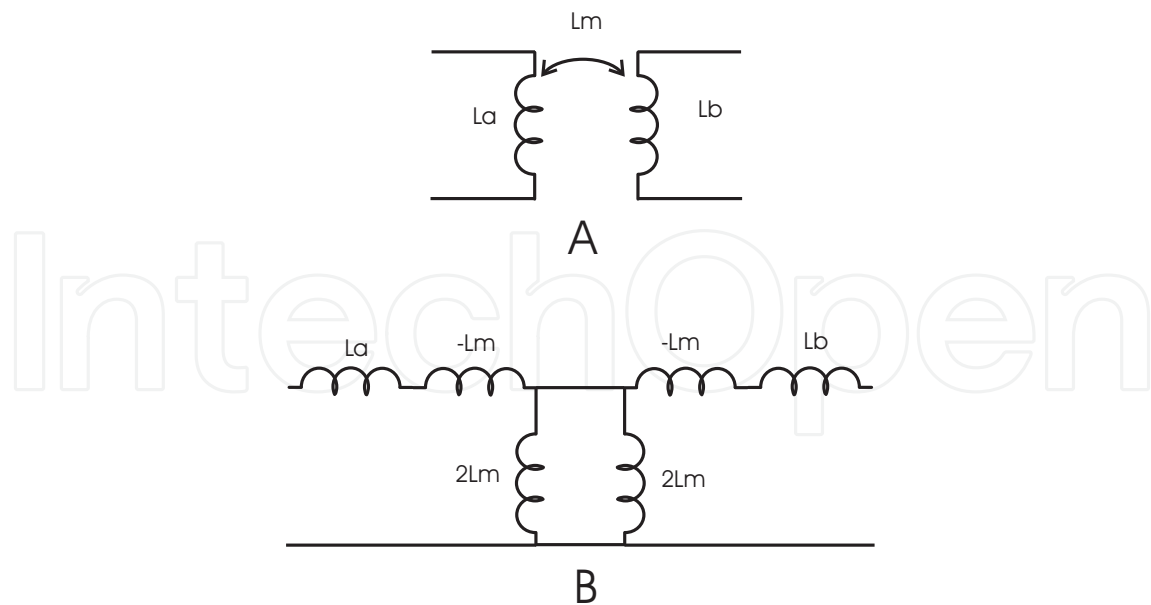


Fig. 4. Equivalent network for the coupled inductors. Representation of coupled inductors in terms of impedance inverter.

the other, will shift the resonant frequency. As a consequence, we need to find an oscillator that is able to keep track of these frequency shifts. It is worthwhile to point out that the latter frequency shifts may occur also when inserting more than one receiving resonators.

2.1.2 Maximum efficiency

It is apparent from eq.(3) that the efficiency depends on the values of Z_S and Z_L . In order to analytically compute the maximum efficiency let us consider the case of identical source and load impedance:

$$Z_L = Z_S = Z_0. \quad (8)$$

With reference to the circuit of Fig. 3 we note that the efficiency now depends only on the reference impedance Z_0 .

The values of L and C depend on the chosen arrangement (i.e. frequency of operation, dimensions of the coils etc.) and are kept fixed; once the value of k is given, it is possible to compute the efficiency. By considering identical resonators and at resonance

$$Z_1 = Z_2 = R \quad (9)$$

we have, from eq. (3)

$$S_{21}(Z_0) = \frac{2j\omega_0 L_m Z_0}{[\omega_0^2 L_m^2 + R^2 + 2RZ_0 + Z_0^2]}. \quad (10)$$

By taking the derivative w.r.t. Z_0 we have:

$$\frac{\partial |S_{21}(Z_0)|}{\partial Z_0} = \frac{2j\omega_0 L_m (R^2 + \omega_0^2 L_m^2 - Z_0^2)}{[\omega_0^2 L_m^2 + R^2 + 2RZ_0 + Z_0^2]^2}. \quad (11)$$

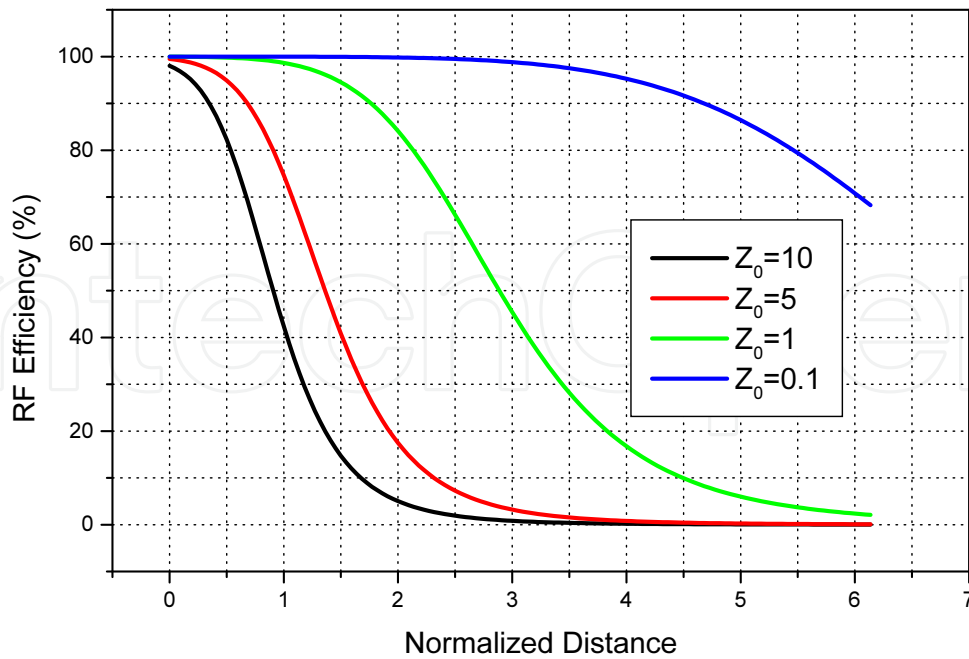


Fig. 5. Computed radio–frequency efficiency (η), for the circuit of Fig. 3, with respect to the normalized distance for various different values of reference impedance Z_0 .

The condition

$$\frac{\partial |S_{21}(Z_0)|}{\partial Z_0} = 0 \tag{12}$$

provides the sought value for the reference impedance:

$$Z_0 = \sqrt{R^2 + \omega_0^2 L_m^2} \tag{13}$$

or equivalently:

$$\omega_0^2 L_m^2 = Z_0^2 - R^2; \tag{14}$$

By inserting the above expression in denominator of eq.(10) we obtain for the S_{21}

$$S_{21} = \frac{j\omega_0 L_m}{[R + Z_0]} \tag{15}$$

which provides:

$$|S_{21}(Z_0)|^2 = \frac{\omega_0^2 L_m^2}{[Z_0 + R]^2} = \frac{[Z_0 - R]}{[Z_0 + R]} \tag{16}$$

In Fig. 5 we have plotted the radio–frequency efficiency (η of (4)) with respect to the normalized distance for various different values of reference impedance Z_0 . It is important to note that high values of efficiency are possible only if the reference impedance is low. This means that, if the distance is fixed, in order to achieve a high efficiency it is appropriate to use matching networks between the generator and the transmitting coil and between the load and the receiving coil, that transform the impedances of the load and generator into suitable values.

2.2 Matching networks

In order to improve the efficiency we have seen that it is appropriate to introduce matching networks between the source and the transmitting resonator and between the receiving resonator and the load. These matching network will adjust the source/load impedance to the impedances necessary to optimize the efficiency. A possible way to realize the matching networks is by inserting impedance inverters before the load impedance and after the source impedance; by doing so we recover the equivalent network shown in Fig. 6.

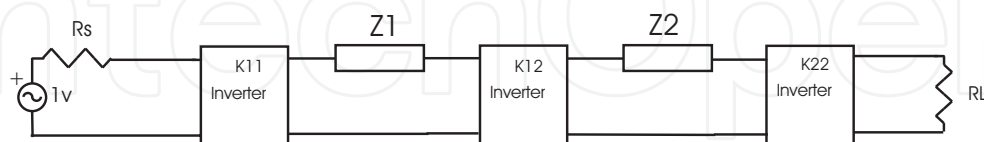


Fig. 6. Narrowband circuit model using impedance inverters; note the presence of the couplings K_{11} and K_{22} to model the input and output loop coupling to the resonator .

Impedance inverters can be realized in a variety of ways. As an example, let us recall the equivalences reported in Fig. 7, Fig. 8, where it is shown that immittance inverters can be represented, over a narrow band, in terms of inductive or capacitive networks.

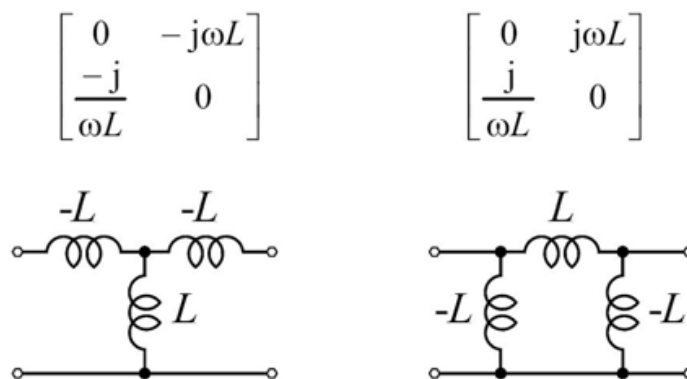


Fig. 7. Realization of immittance inverters in terms of inductive networks. The corresponding ABCD matrices are also reported.

An alternative approach may also be employed, by using the same resonant coils also as matching networks. In fact, with reference to Fig. 9, we note that we have connected the coaxial center line at a certain distance from the end of the coil, thus splitting the inductance. It may be noted that the equivalences reported in Fig. 10 may be used. Therefore, also in this case, the representation in terms of immittance inverters can be used. We can therefore conclude that a fairly general network model for representing WRELS is the one reported in Fig. 6.

One possible physical realization is e.g. that shown in Fig. 2; the latter is composed of four coils and two capacitors in a symmetrical structure. We have used 2 mm gauge silver plated wire to wind the coils and two 330 pF silvered mica capacitors to realize the resonators. The input and output coils are 65mm diameter single loops, while the resonator coils are 2 turn, 60 mm diameter, 22 mm length coils. The resonator and the input loops are placed on plastic stands for their positioning.

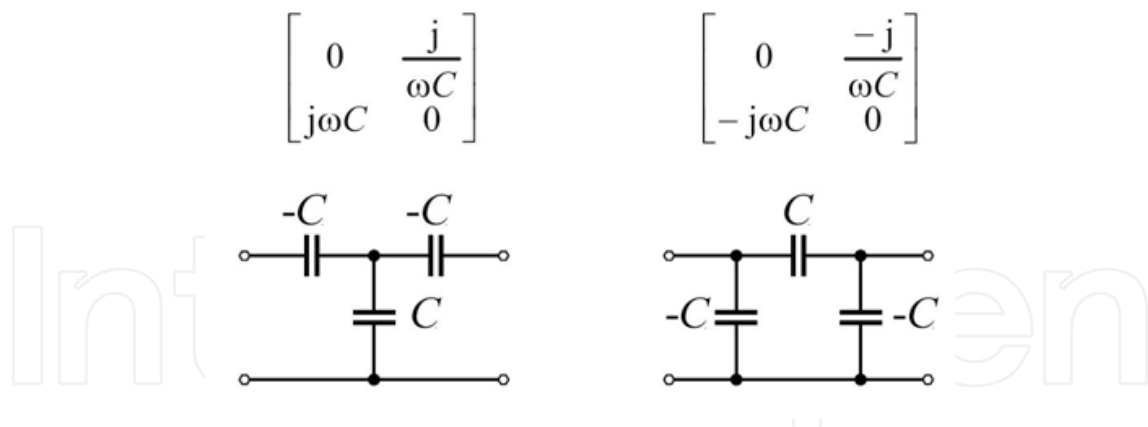


Fig. 8. Realization of immittance inverters in terms of capacitive networks. The corresponding ABCD matrices are also reported.

It is worthwhile to point out that a rigorous model of the structure in Fig. 2, would have required to take into account also all the couplings between all the resonators. A rigorous network for this situation will be illustrated in sec. 3. For the moment, it suffice to say that the network of Fig. 6 is a very good approximation and applicable for the design of the input/output coupling sections.

Note that inductive or capacitive networks can also be used to shift the resonant frequencies.

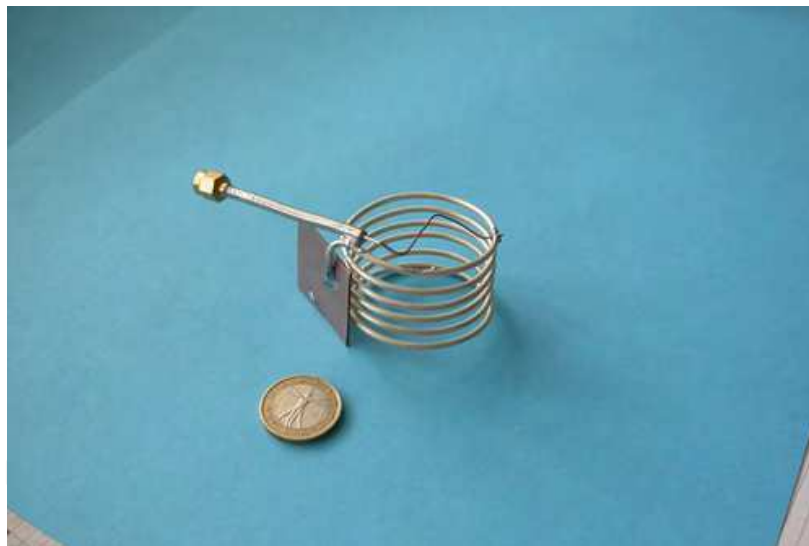


Fig. 9. The coaxial input placed along the helix provides a splitting of the inductance that can be used for matching purposes, thus avoiding the use of additional transformers.

2.3 Narrow band analysis of coupled resonators systems

The equivalent network shown in Fig. 6 can be analyzed in a very simple way by using ABCD matrices. We consider coupled resonators identified by their couplings, Q factors, and resonance frequency; we may express the impedance Z_1 and Z_2 in terms of the resonant frequency $\omega_0 = \frac{1}{\sqrt{LC}}$, unloaded Q factor, and resonator reactance slope parameter $\chi = \sqrt{\frac{L}{C}}$, as follows:

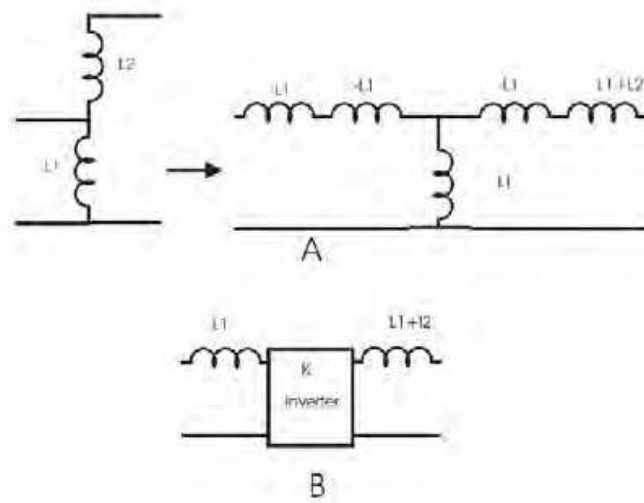


Fig. 10. Equivalent network showing how a splitted inductance can be represented in terms of immittance inverters.

$$Z_{1,2} = \chi_{1,2} \left[j \left(\frac{\omega}{\omega_0} - \frac{\omega_0}{\omega} \right) + \frac{1}{Q_{1,2}} \right]. \quad (17)$$

The inductors' couplings can be modelled as impedance inverters whose value is:

$$K = \omega L_m = \omega k_{ab} \sqrt{L_a L_b}, \quad (18)$$

where L_m is the mutual inductance and k_{ab} the inductive coupling coefficient, L_a and L_b the inductances of the coupled inductors.

The ABCD matrix of a impedance inverter can be written as follows:

$$\begin{bmatrix} 0 & -jK \\ \frac{-j}{K} & 0 \end{bmatrix}, \quad (19)$$

while for a series impedance Z we have:

$$\begin{bmatrix} 1 & Z \\ 0 & 1 \end{bmatrix}. \quad (20)$$

We can express the input-output ABCD matrix \mathbf{T}_{ABCD} of the cascade of impedance inverters and series impedance of Fig. 6 by the following matrix product:

$$\mathbf{T}_{ABCD} = \begin{bmatrix} A & B \\ C & D \end{bmatrix} = \begin{bmatrix} 1 & Z_s \\ 0 & 1 \end{bmatrix} \cdot \begin{bmatrix} 0 & -jK_{11} \\ \frac{-j}{K_{11}} & 0 \end{bmatrix} \cdot \begin{bmatrix} 1 & Z_1 \\ 0 & 1 \end{bmatrix} \cdot \begin{bmatrix} 0 & -jK_{12} \\ \frac{-j}{K_{12}} & 0 \end{bmatrix} \cdot \begin{bmatrix} 1 & Z_2 \\ 0 & 1 \end{bmatrix} \cdot \begin{bmatrix} 0 & -jK_{22} \\ \frac{-j}{K_{22}} & 0 \end{bmatrix} \cdot \begin{bmatrix} 1 & Z_L \\ 0 & 1 \end{bmatrix}. \quad (21)$$

The elements of the ABCD matrix \mathbf{T}_{ABCD} are the following:

$$\begin{aligned} A &= \frac{j[Z_2 K_{11}^2 + Z_s K_{12}^2 + Z_1 Z_2 Z_s]}{K_{11} K_{12} K_{22}} \\ B &= \frac{j[K_{11}^2 K_{22}^2 + Z_2 Z_L K_{11}^2 + Z_L Z_s K_{12}^2 + Z_1 Z_s K_{22}^2 + Z_1 Z_2 Z_L Z_s]}{K_{11} K_{12} K_{22}} \\ C &= \frac{j[K_{12}^2 + Z_1 Z_2]}{K_{11} K_{12} K_{22}} \\ D &= \frac{j[Z_L K_{12}^2 + Z_1 K_{22}^2 + Z_1 Z_2 Z_L]}{K_{11} K_{12} K_{22}} \end{aligned} \quad (22)$$

By transforming the ABCD matrix to the scattering matrix, and by considering S_{21} , we obtain:

$$|S_{21}|^2 = \left| \frac{2\sqrt{R_s R_L}}{A \cdot R_s + B + C \cdot R_s R_L + D \cdot R_s} \right|^2. \quad (23)$$

Equation (23) gives the efficiency of the network when R_s and R_L are respectively the source and load impedance. It is apparent that, from (17) and (23), we can express the power transmission efficiency in terms of the resonators parameters and their couplings.

When considering a symmetrical system, where we have two identical resonator ($Z_1 = Z_2 = Z$), and symmetrical couplings ($K_{11} = K_{22} = K$), eq. (21) can be simplified as follows:

$$\begin{aligned} A &= \frac{j[K^2 + Z_s K_{12}^2 + Z_{in}^2]}{K^2 K_{12}} \\ B &= \frac{j[K^2 + 2 \cdot Z \cdot Z_{in} K^2 + Z_{in}^2 K_{12}^2 + Z^2 \cdot Z_{in}^2]}{K^2 K_{12}} \\ C &= \frac{j[K_{12}^2 + Z^2]}{K^2 K_{12}} \\ D &= \frac{j[Z_{in} K_{12}^2 + Z K^2 + Z_{in} Z^2]}{K^2 K_{12}} \end{aligned} \quad (24)$$

and eq. (23), with input and output reference impedance R , simplifies into:

$$|S_{12}|^2 = \left| \frac{2R}{A \cdot R + B + C \cdot R^2 + D \cdot R} \right|^2. \quad (25)$$

2.4 Input and output coupling design

Let us consider the equivalent network of the WREL system shown in Fig. 6; while the coupling k_{12} between the resonators coils is dependent on their distance and dimensions, the input-output couplings must be designed in order to maximize $|S_{21}|^2$. Input and output impedances, denoted respectively by R_s and R_L , are in general different; also loop resonator resistances R_1 and R_2 may be different. Note that at resonance $Z_1 = R_1$ and $Z_2 = R_2$; in this case it is straightforward to transfer the output impedance at the input port, giving:

$$R_{in} = \frac{K_{11}^2}{R_1 + \frac{K_{12}^2}{R_2 + \frac{K_{22}^2}{R_L}}}, \quad (26)$$

where K_{11} and K_{22} are, respectively, the input and output inverters values; R_1 and R_2 the loop resistance of the transmitting and receiving resonator, R_L the load resistance, and K_{12} the inverter corresponding to the coupling of the resonators coils. In particular, we can consider $K_{11} = K_{22}$; the matching condition at the input port is:

$$R_{in} = R_s. \quad (27)$$

It follows from (26) and (27) that:

$$K_{11} = K_{22} = \sqrt{\frac{\frac{R_2 R_L - R_1 R_S}{2} + \sqrt{(\frac{R_2 R_L - R_1 R_S}{2})^2 + 4 R_L R_S (K_{12}^2 - R_1 R_2)}}{2}}. \quad (28)$$

Once the value of the input inverter is obtained it can be realized by different implementations, like coupled inductors, tapped inductors or capacitive networks as described before. If we consider a symmetrical structure where we have $L_1 = L_2$, $Z_1 = Z_2$, $R_s = R_L = R$, from eq. (17) the eq. (28) can be furtherly simplified as follows:

$$k_{11} = k_{22} = \sqrt{\frac{R}{L_1 \omega_0} \sqrt{k_{12}^2 + \left(\frac{1}{Q}\right)^2}}. \quad (29)$$

In the above eq. k_{12} is the inductive coupling coefficient between the resonators, Q the quality factor, ω_0 the resonance frequency and $k_{11} = k_{22}$ are the coupling coefficient of the input-output loops to the resonators. Once the input-output coupling coefficient is calculated, one can compute the distance between the coils centers as in Dionigi & Mongiardo (2010).

2.5 Computation of the network elements

The equivalent network is quite useful for modeling wireless resonant energy links in different conditions, as reported in Dionigi et al. (2009) and Dionigi et al. (2010). Moreover, the values of the network elements can be derived as described in many references (see for example sec. 4.1 of Finkenzeller (2003) or Grover (2004) for inductance calculations). In particular, the coil inductance, expressed in μH , of total length L_e , diameter D (expressed in meters), and N turns, can be written as:

$$L = \frac{(ND)^2}{(L_e + 0.45D)}. \quad (30)$$

By denoting with R_i the radius of the i -th coil and by H_{12} the distance between the center of resonator 1 and resonator 2, we can compute the magnetic coupling factor K as in Grover (2004):

$$K_{12} = 1.4 \frac{(R_1^2 R_2^2)}{\sqrt{R_1 R_2} \sqrt{(R_1^2 + H_{12}^2)^3}}. \quad (31)$$

Finally, the mutual inductance is computed by:

$$M_{12} = K_{12} \sqrt{L_1 L_2}. \quad (32)$$

2.6 Design of a wireless power transfer system at fixed distance

Fig. 11 illustrates the behavior of the coupling factor k_{12} between two resonant coils as function of the center distance, normalized to the coils diameter. Naturally, the coupling decrease with the distance. Once the value of k_{12} is given, assuming $R = 50\Omega$ and by using (29), it is possible to compute the input coupling coefficients k_{11} and k_{22} . Once the latter coupling coefficients are computed, we can calculate the distance from the input loop of the resonator coil center which

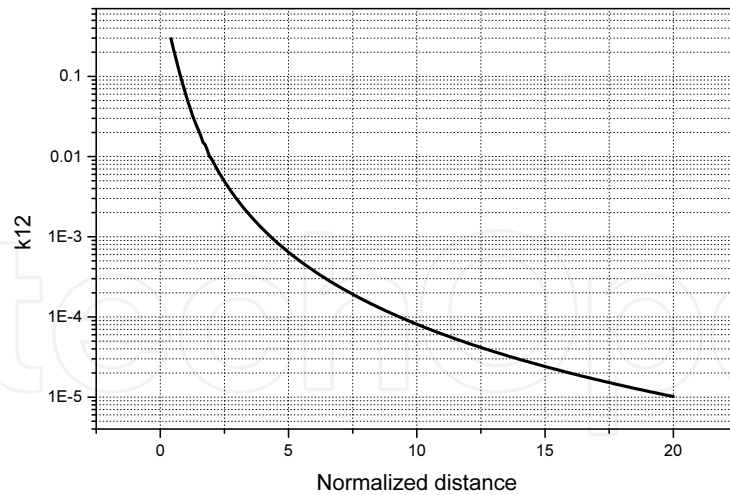


Fig. 11. Coupling coefficient of a 2 turn, 60 mm diameter coil vs center coils distance normalized to diameter.

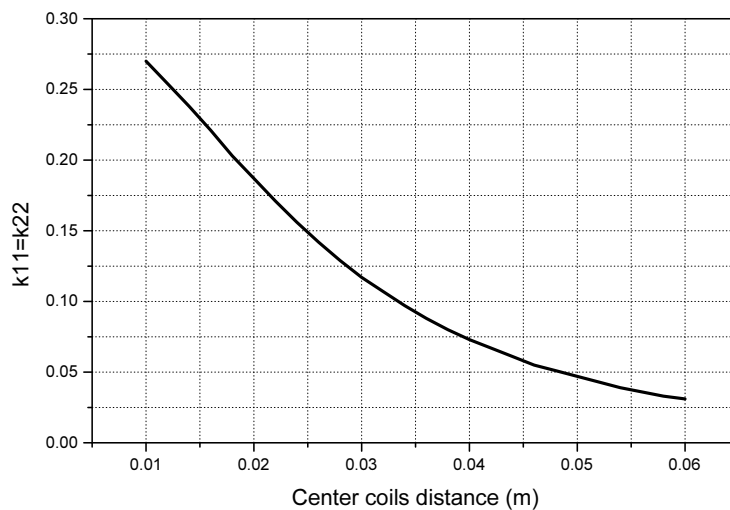


Fig. 12. Input loop and resonator coil coupling coefficient vs center coil distance for 65 mm diameter loop and 2 turn, 60 mm diameter, 22 mm length coil.

realize the sought value. Fig. 12 gives the coupling factor of the input loop to the resonator coil as function of the center distance of the resonator coil.

In Fig. 13 and Fig. 14, the efficiency of the passive, linear part of the system is investigated as function of the distance and resonators Q factor. Note that the proposed design procedure allows, for a given type of resonator, thus for given Q and coupling, to find the maximum efficiency achievable. In addition, as noted in Dionigi & Mongiardo (2011), the design procedure also permits, for a given distance and efficiency, to find the necessary resonator quality factor Q.

As an example, we have designed two study cases by separating the resonators coil centers by 75mm and 100 mm. The calculated input loop inductance is 130 nH. The transmitting/receiving resonators have been designed for operating at a resonant frequency of 14.56 MHz. The measured Q of the resonators is about 300 and the slope parameter is $\chi=33.26 \Omega$. From the design formulas we have calculated the input loop to resonator coil distance of

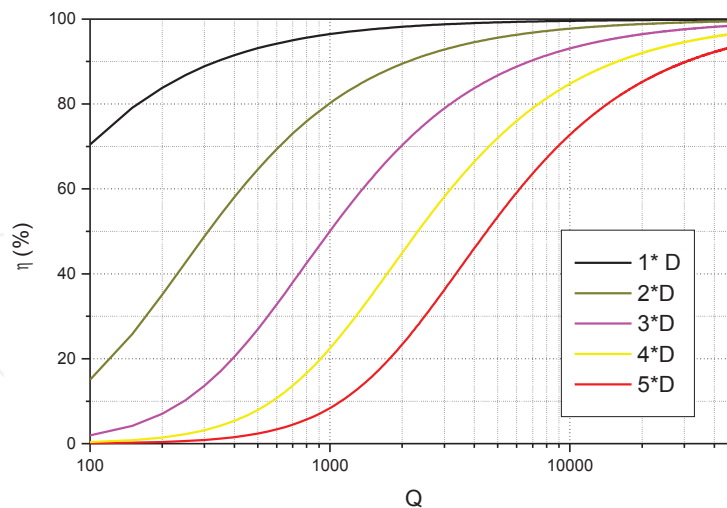


Fig. 13. Computed efficiency for coils diameter $D=60\text{mm}$ at distances of $1D-5D$, as function of Q factor.

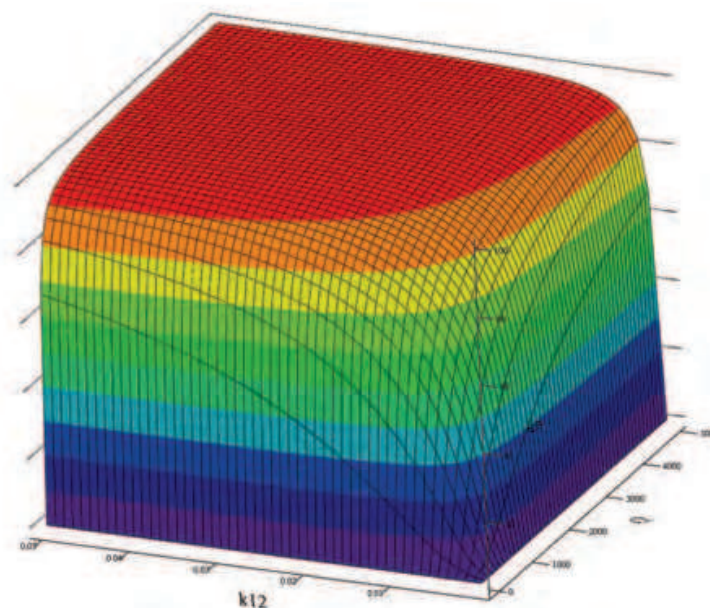


Fig. 14. Computed efficiency as a function of the Q and of the coupling.

15 mm and 25mm, respectively. The scattering parameters of the structure has been measured by a vector network analyzer (agilent PNA n5230A) assuming input and output impedance $R = 50\Omega$. In Fig. 15 are reported the calculated and measured efficiency of the coupled resonator system; it is possible to observe a fairly good agreement. It can be also noted that, at 100mm distance, it is not possible to reach very high efficiency values; this is mainly due to the low Q factor of the resonators. It is clear from the theory that higher transmission efficiencies can be reached only if very high Q resonators are used (see also Dionigi & Mongiardo (2011)). As a further example, the structure of Fig. 16 has been optimized for WPT at different distances. The system is composed of a pair of resonator made of a single loop inductor of diameter 20 cm and a couple of capacitors made of two rectangular pieces of high quality teflon substrate metallized on both sides. In this way a high quality capacitor is obtained.

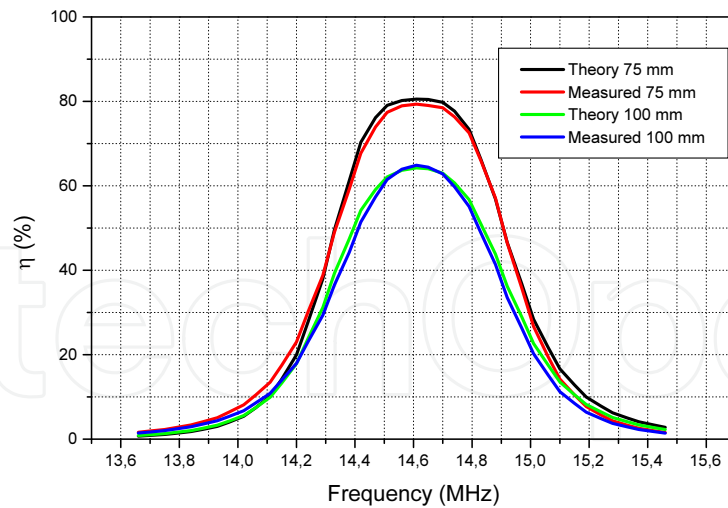


Fig. 15. Simulated and measured efficiency at 75 and 100 mm resonators coils center distance.

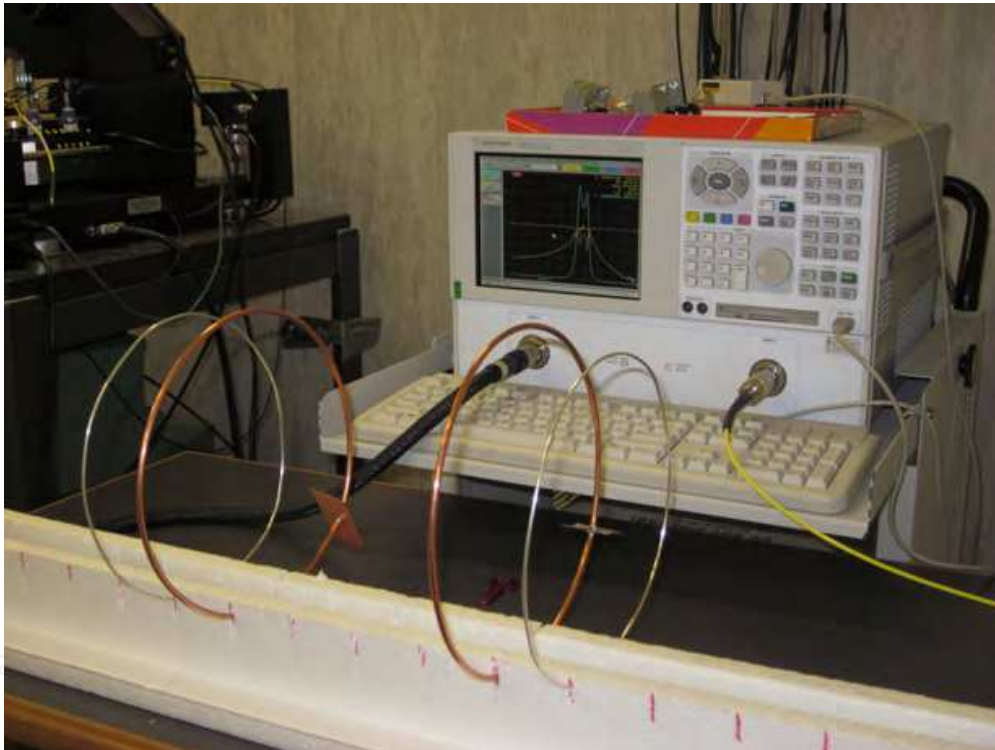


Fig. 16. A resonant WPT link with matching networks.

The teflon substrate is a taconic TLY5 with thickness of 0.51mm. A capacitance of about 72 pF is easily obtained, and, by trimming the edge of the substrate, an accurate tuning of the resonators is obtained. The system has been tuned and measured. In Fig. 17 -Fig. 18 and 19 we have reported the efficiencies of the linear part as obtained by using a Vector network analyzer.

Due to the resonators quality factor of about 350 a high efficiency is obtained at a distance of 10 cm. In this configuration the linear part of the WPT system delivers the power to the load almost like a direct connection. As the distance between the two resonators increases a drop

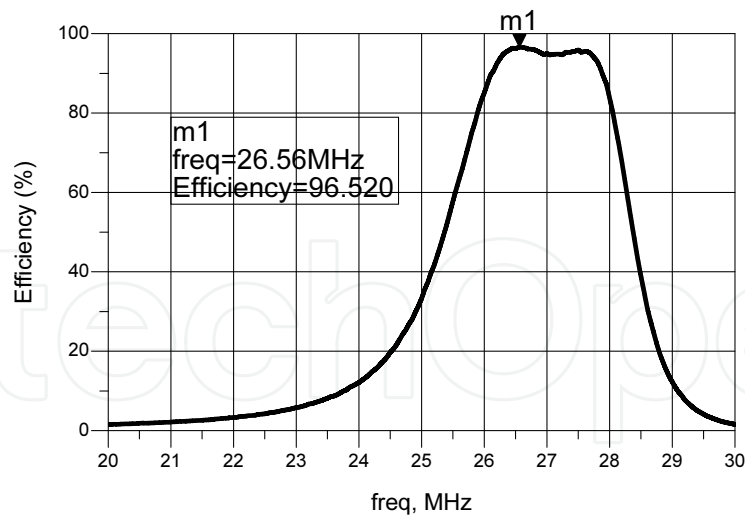


Fig. 17. Measured efficiency at 10 cm resonators coils center distance; the corresponding normalized distance is 0.5. The normalized distance is defined as the ratio between the coils distance and their diameter.

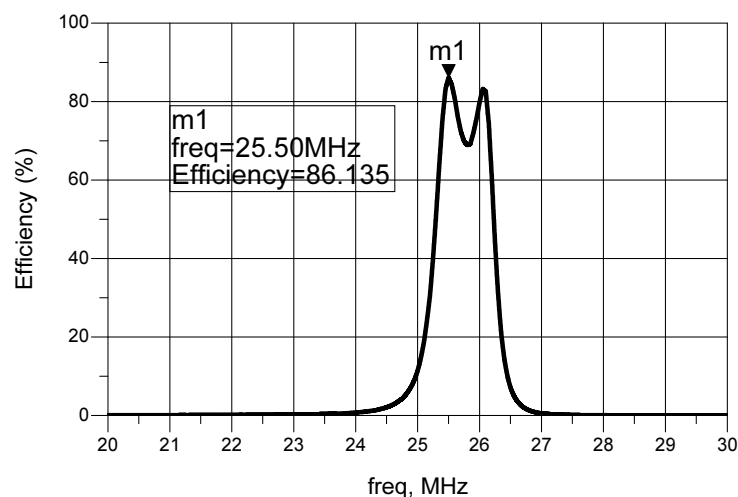


Fig. 18. Measured efficiency at 20 cm resonators coils center distance; the corresponding normalized distance is 1.

of the efficiency is measured, although at the distance of 30 cm an efficiency of about 77% is reached.

3. General analysis of WRELS

3.1 The general network model for coupled resonators

A more general analysis technique can be adopted when multiple resonators are employed. In this case, cross coupling between resonators is possible and a more accurate analysis can be implemented. In Fig. 20, as an example, three mutually coupled inductors are shown. An equivalent network of the structure of Fig. 20 is illustrated in Fig. 21.

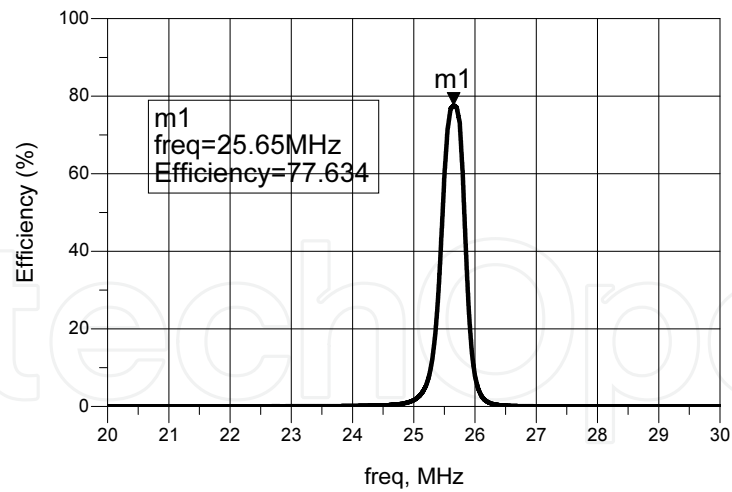


Fig. 19. Measured efficiency at 30 cm resonators coils center distance; the corresponding normalized distance is 1.5.

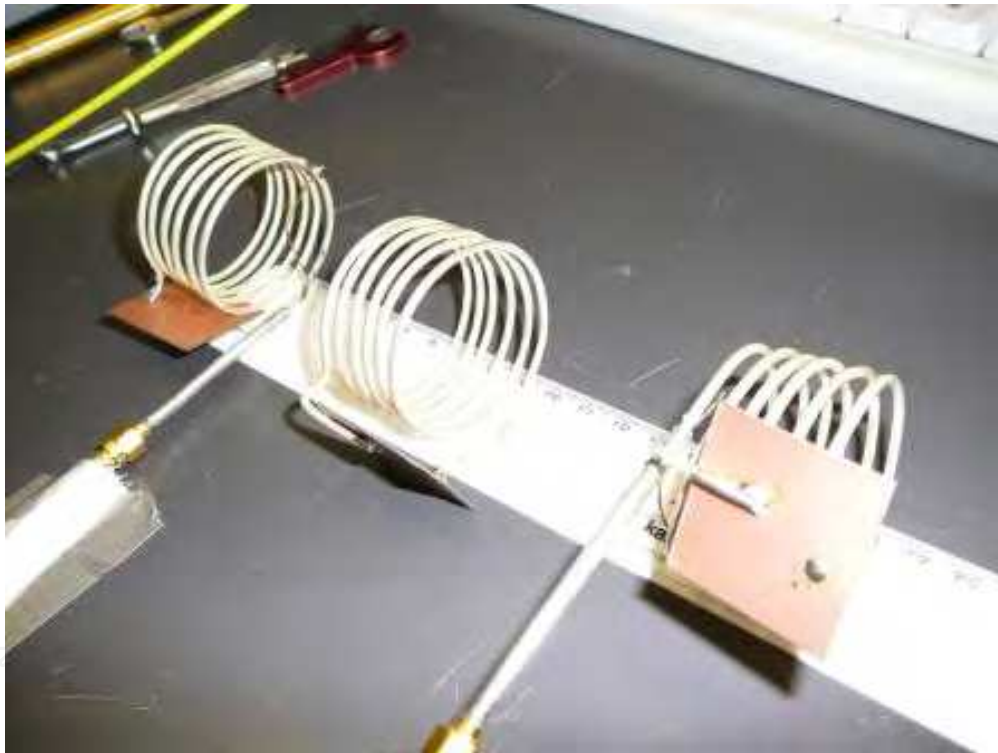


Fig. 20. Photograph of resonant conducting wire loops: the first and last resonator are, respectively, the source and the load. The resonator in the middle extends the operating range.

We can compute the solution of the circuit of Fig. 21 in the standard manner. By defining the impedance Z_i with $i = 1, 2, 3$ as

$$Z_i = j \left(\omega L_i - \frac{1}{\omega C_i} \right) + R_i \quad (33)$$

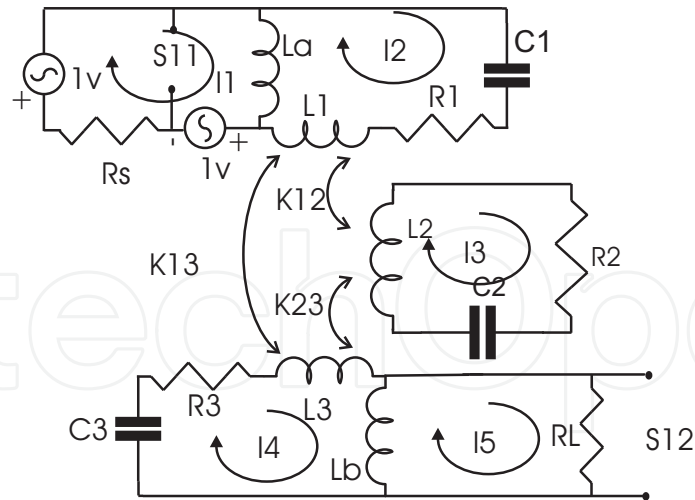


Fig. 21. Equivalent network of the wireless resonant energy link configuration shown in the previous figure.

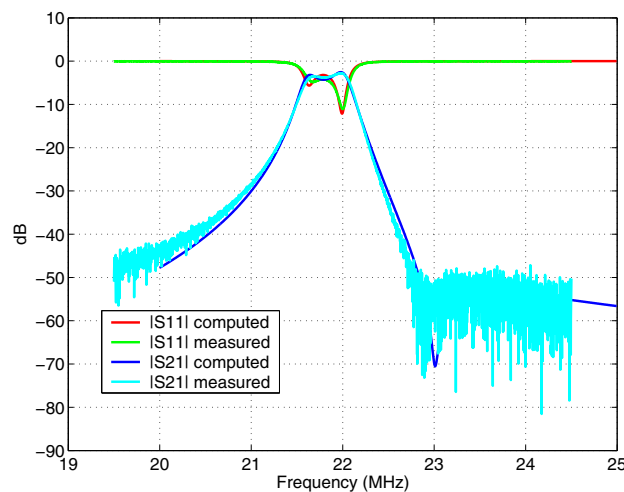


Fig. 22. Reflection and transmission coefficient of the circuit with three resonators.

and by calling with A the system matrix and with I the currents vector we can write:

$$A \cdot I = \begin{bmatrix} j\omega L_a + R_s & -j\omega L_a & 0 & 0 & 0 \\ -j\omega L_a & Z_1 & j\omega M_{12} & j\omega M_{13} & 0 \\ 0 & j\omega M_{12} & Z_2 & j\omega M_{23} & 0 \\ 0 & j\omega M_{13} & j\omega M_{23} & jZ_3 & -j\omega L_b \\ 0 & 0 & 0 & -j\omega L_b & j\omega L_b + R_L \end{bmatrix} \begin{bmatrix} I_1 \\ I_2 \\ I_3 \\ I_4 \\ I_5 \end{bmatrix} = \begin{bmatrix} 2 \\ 0 \\ 0 \\ 0 \\ 0 \end{bmatrix} \quad (34)$$

For scattering parameters computation it is possible to use the excitation scheme shown in Fig. 21 with two 1 V generators; by considering this arrangement we have:

$$S_{11} = 1 + I_1 R_s; S_{21} = -I_5 R_L \quad (35)$$

The measured and calculated response of the circuit of Fig. 21 is shown in Fig. 22. It is apparent that a direct coupling between the input resonator and the output one adds a transmission zero to the transmission coefficient.

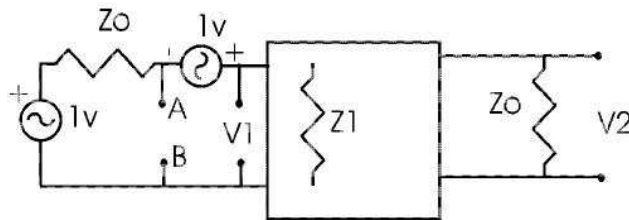


Fig. 23. Equivalent network for spice computation of scattering parameters.

The analysis of a multicoil system can be obtained extending eq.s (34-35). In the general case no assumption can be made on the mutual couplings of the different coils. This affects the solution matrix producing non zero elements above and below the second diagonal row. Discarding the capacitive coupling the solution matrix elements can be written as follows:

$$A_{i,k} = \begin{cases} -j\omega M_{i,k} & \text{if } i \neq k \\ j \left[\omega L_i - \frac{1}{\omega C_i} \right] + R_i. & \text{if } i = k \end{cases} \quad (36)$$

This methodology, although well known, paved the way to the analysis and optimization of very complex structures that may arise from the necessity of extending the range of a WPT system while controlling the field values.

3.2 Spice computation of scattering parameters

With reference to the circuit illustrated in Fig. 21, our goal is to obtain a characterization of the circuit. A simple modification of the input section allows us to find out the scattering parameters directly from spice computations. By considering Fig. 23 and by denoting with Z_0 the reference impedance, we have

$$S_{11} = \frac{Z_1 - Z_0}{Z_1 + Z_0} \quad (37)$$

and

$$V_1 = 2 \frac{Z_1}{Z_1 + Z_0}. \quad (38)$$

By solving the above eq. for Z_1

$$Z_1 = 2 \frac{V_1 Z_0}{2 - V_1}, \quad (39)$$

and, by substituting into (37), we obtain:

$$S_{11} = V_1 - 1 \quad (40)$$

From the circuit in Fig. 23 it is apparent that the voltage between points A and B provides the scattering parameter S_{11} .

Concerning S_{21} we have:

$$S_{21} = \frac{V_2 - I_2 Z_0}{V_1 + I_1 Z_0}. \quad (41)$$

When the port 2 is terminated by its reference impedance the following relationship holds:

$$I_2 = -\frac{V_2}{Z_0}, \quad (42)$$

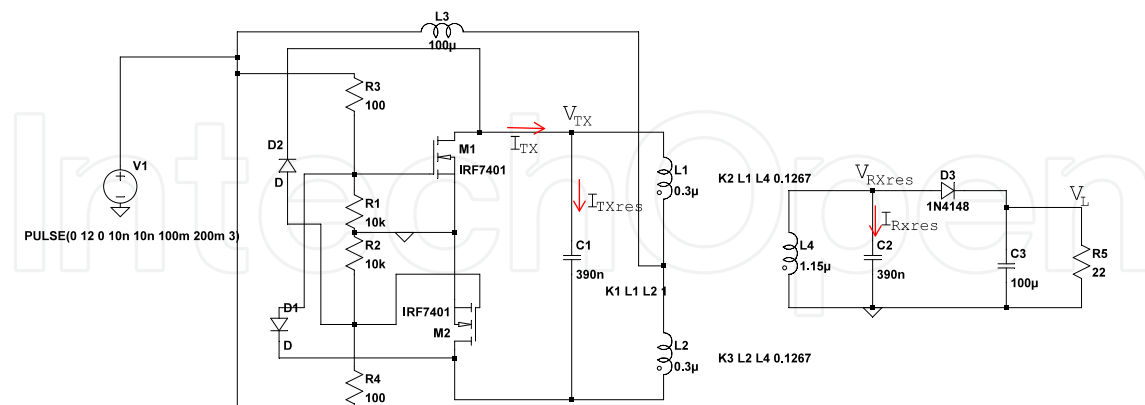


Fig. 24. Power driving unit schematic, based on a Royer oscillator.

which yields:

$$S_{21} = 2 \frac{V_2}{V_1 + I_1 Z_0}. \quad (43)$$

By considering that:

$$I_1 = \frac{V_1}{Z_1} \quad (44)$$

we get:

$$S_{21} = 2 \frac{V_2}{V_1} \frac{1}{1 + Z_0/Z_1} \quad (45)$$

which, after substitution of (39) into (44), provides the sought result:

$$S_{21} = V_2 \quad (46)$$

By using the above formulation it is possible to obtain an accurate frequency domain and time domain analysis of the circuit by using a standard spice simulator.

4. Design of the power driving unit of the wireless link

A crucial block of an inductive power link system is the external power driving unit. Usually, class E power amplifiers are employed; unfortunately, they require square pulses to drive the circuit which, in turn, may affect the optimum value of the power added efficiency (PAE). A power oscillator is therefore a better choice and it is designed to simultaneously ensure high efficiency and higher harmonics rejection. A possible equivalent circuit topology is schematically reported in Fig. 24. It consists of a differential power oscillator formed by combining a cross-coupled MOSFET structure with a resonant load network. The latter is used as the primary side link coil of the power link system. For power transfer a secondary resonator is used, and is also reported in Fig. 24. The entire link of Fig. 24 is considered for the oscillator analysis to account for the variation of the coupling strength with coils distance

D(mm)	K12	f_{osc} (KHz)	P_{DC} (W)	V_{TX} (V)	I_{TXres} (A)	V_{RXres} (V)	I_{RXres} (A)	V_L (V)	P_L (W)
50	0.3426	201.50	53.70	36.80	20.00	34.50	18.30	27.00	33.20
100	0.1267	225.00	43.50	36.80	20.40	28.60	18.44	23.10	24.30
150	0.0603	230.30	19.60	36.70	21.60	16.50	9.40	12.40	7.06
200	0.0334	230.80	12.00	36.50	21.00	9.50	5.40	6.80	2.13
300	0.0133	231.00	9.00	36.70	21.00	4.40	2.35	2.60	0.31

Table 1. Circuit simulated currents voltages and power.

when determining the oscillator actual load. In this way its nonlinear operating regime and oscillation frequency may be computed. At the oscillator side, the source resonator is represented by a resonant circuit (L1,L2,C1). This circuit couples with the secondary resonator (L4,C2) via the magnetic field in free-space (the electric field being mainly confined in the lumped capacity). Thus, the coupling behaviour is described in terms of the inductances L1, L2 and L4 and their mutual coupling K2 and K3.

A circuit level non linear analysis of the oscillator regime may be carried out by time-domain simulation or by means of the Harmonic Balance technique, specialized for autonomous circuits Rizzoli (1994). In the latter case, harmonic content of the oscillator waveforms and the actual frequency dependence on the linear subnetwork are accounted for with no limitations. Oscillator steady state regimes for varying distances between primary and secondary coils are then computed together with the associated output power and conversion efficiency. The linear embedding network is either described by rigorous EM analysis or by the equivalent circuit representation previously discussed in this chapter, at all the frequencies of interest, up to the harmonic order needed to accurately describe the oscillator nonlinear regime. For the case study considered here, the primary coil inductance L_p , expressed in μH , with a total length L_e , diameter D (expressed in meters), and N turns, may be modelled by using eq.(30). By denoting with r_i the radius of the i -th coil and by d_{12} the distance between the center of the primary and secondary resonators, the magnetic coupling factor K may be predicted using eq.(31).

The Q factor of the inductor is included in its circuit model to predict the effective load network. The most significant quantities resulting from simulations of the entire power transmission system, are summarized in Table 1 for varying distances between coils; the corresponding coupling factor K_{12} , is also reported in the same table for clarity. For the present analysis the supply voltage is fixed at 12V and a reference system load of 22 Ohm is considered. From the computed DC current (I_{DC}), the oscillator power consumption (P_{DC}) is derived. The phasors of the output voltages and currents, V_{TX} and I_{TX} , at oscillation frequency, are used to predict the transmitter output power, the power entering transferred to the oscillator load. As expected, V_{TX} is proportional to the supply voltage and does not significantly vary with the coil distances and thus with the system load. For completeness currents and voltages in the secondary resonator (I_{TXres} , I_{RXres}) and the current in the primary one I_{TXres} , are reported in the same table too.

The system dependence on the coils distances and on the coupling factor is evident from the voltages and currents phasors of the receiver resonator branches, V_{RX} and I_{RX} , and of the load branch, V_L and I_L . By means of these quantities the system efficiency, computed as:

$$\eta_{osc}(\%) = \frac{P_L}{P_{DC}} \quad (47)$$

may be quantified and plotted as in Fig. 26. It can be observed that the transmission efficiency is a nonlinear function of the transmitter and receiver distance and can only be predicted by the simultaneous co-design of the power oscillator and of the coupling resonators. For example, it is interesting to note that transmission efficiency depends on the intensity of the H field. This dependence tells us that, in order to have high efficiency, we have to position the receiver in the high H field intensity zone of the transmitter. Once again, the current flowing in the transmitting resonant circuit, I_{TXres} , is also used to evaluate the magnetic field produced by the transmitting coil in the axial position. In particular, we can calculate the value of the magnetic field along the axis at the center of the coil by using the following expression:

$$H = \frac{I_{TXres} N r^2}{(2(r^2 + d^2))^{3/2}} \quad (48)$$

where I_{TXres} is the current in the coil, N is the number of turns, r the radius of the coil and d the distance of the observation point along the coil axis from the center of the coil. Measured and computed values of the magnetic field are compared in Fig. 27.

Previous results may be used as a suitable starting point for a dedicated system design in a specific application environment. For example, once the range of primary and secondary coil distances is established, the desired oscillator band is derived and a broadband optimization may be carried out to enhance the starting point performances in terms of output power and conversion efficiency. These quantities directly determine the efficiency of the entire wireless power transmission system. Design variables may be the DC voltage range and the oscillator linear embedding network, including geometrical parameters of the primary and secondary coils.

For the setup shown in Fig. 25, the resonant coils are made of a 2 turn silver-plated wire with 3 mm gauge wounded with 180 mm diameter, the coils length are about 30 mm. For the starting point system analysis, both coils are connected in parallel with a 390 pF polypropylene capacitor. Their lengths may be adjusted to tune the resonant frequencies.

5. Resonators' quality factor measurement

5.1 Measuring resonant frequency and Q factor

The measurement of the resonant frequency and Q factor of resonators is based principally on two techniques, namely the reflection method and the transmission method (see e.g. pag. 53 and following of Kajfez (1998)). It is interesting to note that it is not possible to measure directly the unloaded Q of a resonator but only its loaded Q. This is due to the necessity to couple the resonator to an external circuitry in order to pick the measurement signal. However, a simple modeling of the test structure allows one to de-embed the unloaded Q from the measured loaded Q.

In Fig. 28 an equivalent circuit of a resonator, composed by L_2, C_2 and R_2 , coupled to a measuring probe, is described. The measuring probe construction depends on the characteristics of the resonator. In order to measure the Q of a resonator for wireless power transfer, a simple inductive loop is sufficient.

By introducing $\omega_0 = \frac{1}{\sqrt{L_2 C_2}}$ and $Q_0 = \frac{\omega_0 L_2}{R_2}$, the input impedance Z_i at the probe port is given by:



Fig. 25. Photograph of the transmitting circuit and the resonant conducting wire loops together with one euro coin. Note that the resonant coil is excited at its center.

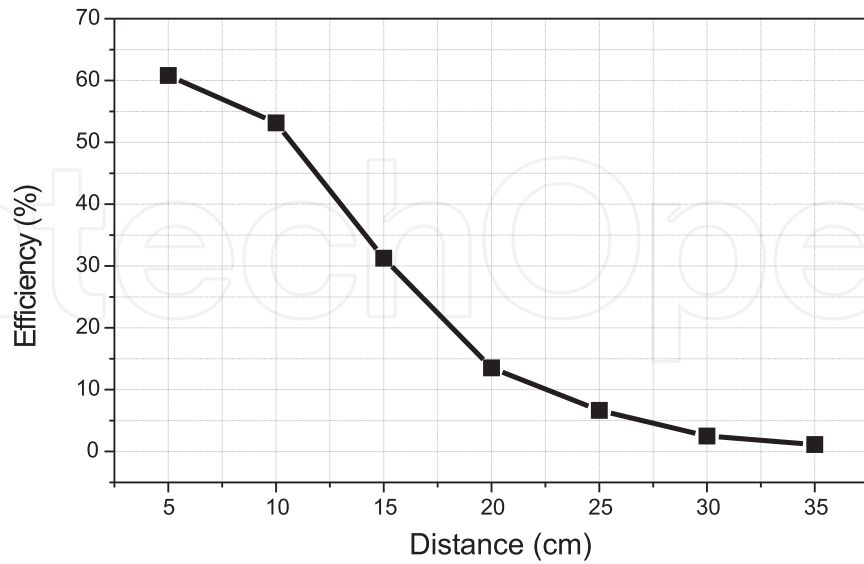


Fig. 26. Computed power transmission efficiency defined as the ratio of the power delivered to the 22 Ohm resistor and the power drawn from the 12 V power supply.

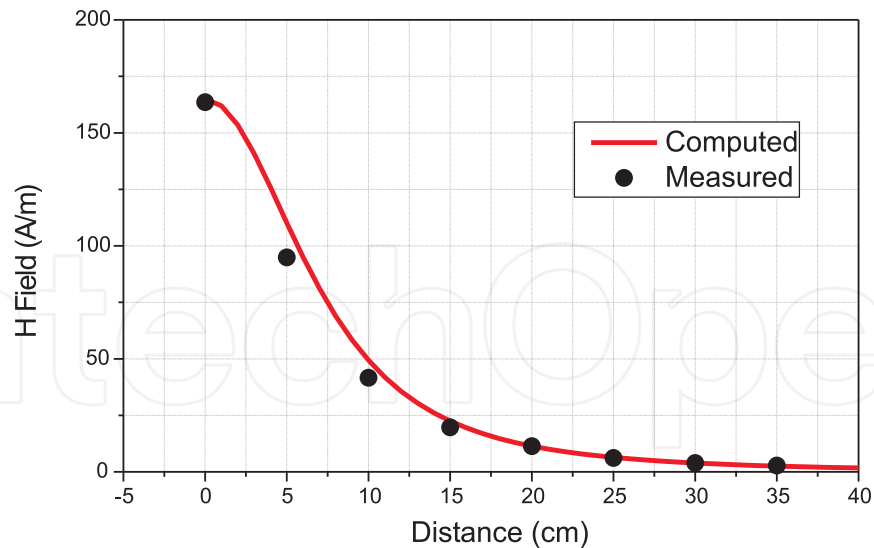


Fig. 27. Measured and computed values of the magnetic field long the axis at the center of the coil.

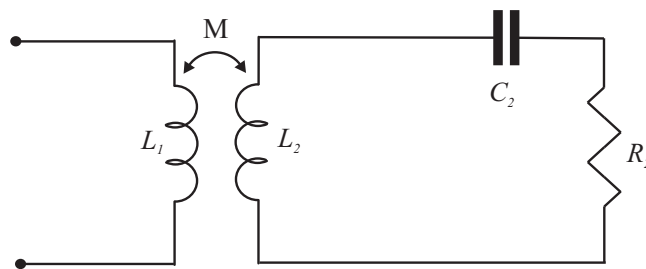


Fig. 28. Equivalent circuit of a resonator (on the right side) coupled to a measuring probe (left side).

$$Z_i = j\omega L_1 + \frac{\frac{(\omega M)^2}{R_2}}{1 + jQ_0 \left(\frac{\omega}{\omega_0} - \frac{\omega_0}{\omega} \right)}. \quad (49)$$

By choosing a small reactance value ωL_1 , we can neglect it, and, at the resonant frequency, the input impedance is given by:

$$Z_i = R_i = \frac{(\omega M)^2}{R_2}. \quad (50)$$

It is convenient to further simplify the frequency dependance as follows:

$$\frac{\omega}{\omega_0} - \frac{\omega_0}{\omega} \simeq 2 \frac{\omega - \omega_0}{\omega_0}; \quad (51)$$

accordingly, eq. (49) can be rewritten as follows:

$$Z_i = \frac{R_i}{1 + jQ_0 2 \frac{\omega - \omega_0}{\omega_0}} \quad (52)$$

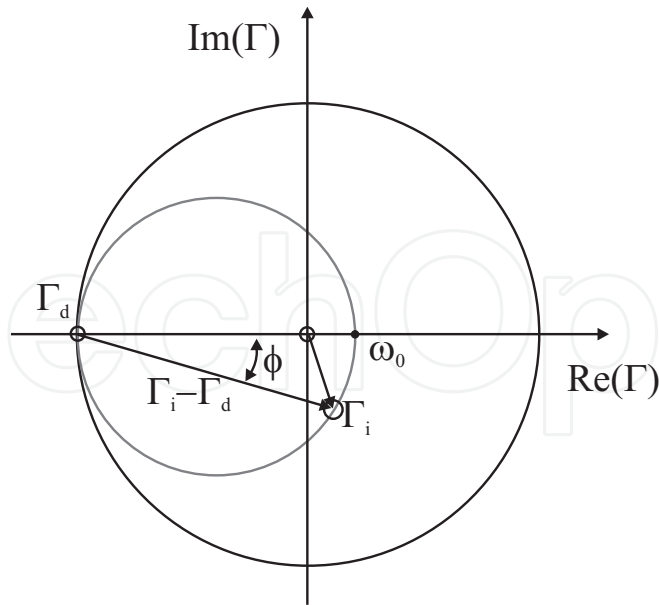


Fig. 29. Reflection coefficient versus ω .

with the corresponding input reflection coefficient expressed as:

$$\Gamma_i = \frac{Z_i - R_c}{Z_i + R_c} \tag{53}$$

where R_c is the reference impedance of the probe port. When we consider a resonant frequency $\omega \rightarrow \infty$ we detune the resonator and the input impedance becomes $Z_i = 0$; the reflection coefficient Γ_d for the detuned resonator becomes $\Gamma_d = -1$.

If we consider the complex number $\Gamma_i - \Gamma_d$, it can be expressed by the following eq.:

$$\Gamma_i - \Gamma_d = \frac{2 \frac{R_i}{R_c}}{1 + \frac{R_i}{R_c} + jQ_0 2 \frac{\omega - \omega_0}{\omega_0}} \tag{54}$$

Given $\kappa = \frac{R_i}{R_c}$ it is clear that it represents the ratio of the power dissipated in the internal resistance and that transmitted to the output port; by denoting with Γ_{ir} the reflection coefficient at resonance, we have:

$$\Gamma_{ir} - \Gamma_d = \frac{2\kappa}{1 + \kappa} \tag{55}$$

which is a real number. A graphical representation of $\Gamma_i - \Gamma_d$ is illustrated in Fig. 29.

As shown in Kajfez (1998), the following relation holds for loaded and unloaded Q:

$$Q_L = \frac{Q_0}{1 + \kappa} \tag{56}$$

and eq.(54) can be rewritten as follows:

$$\Gamma_i - \Gamma_d = \frac{2}{\left(1 + \frac{1}{\kappa}\right) \left(1 + jQ_L 2 \frac{\omega - \omega_0}{\omega_0}\right)} \tag{57}$$

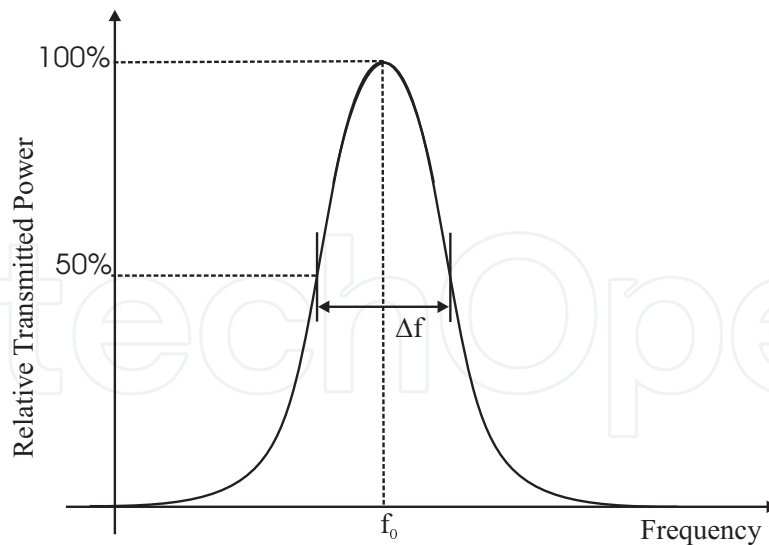


Fig. 30. An example of a measured transmission coefficient.

If we consider the angle ϕ in Fig. 29, we can compute the loaded quality factor Q_L . It can be observed that:

$$\tan(\phi) = -Q_L 2 \frac{\omega - \omega_0}{\omega_0} \quad (58)$$

In order to measure Q_L , one may select two frequencies, denoted by f_3 and f_4 , where $\phi = -45^\circ$ and $\phi = 45^\circ$, respectively, thus obtaining:

$$Q_L = \frac{f_0}{f_3 - f_4} \quad (59)$$

Finally, once κ is computed from eq. (55), we have the value of the unloaded Q:

$$Q_0 = Q_L(1 + \kappa). \quad (60)$$

5.1.1 The two port method

The two port measurement can be easily obtained from the previous formulation by considering, instead of the reflection coefficient, the transmission coefficient between two coupled probes. An example of a measured transmission coefficient is given in Fig. 30.

In this case, the relation between the loaded and unloaded Q is the following Kajfez (1998):

$$Q_L = \frac{Q_0}{1 + \kappa_1 + \kappa_2} \quad (61)$$

where κ_1 and κ_2 depend on the input and output coupling.

It is possible to measure the loaded Q factor from the relative transmitted power by simply computing the ratio between the resonant frequency and the half relative power bandwidth as follows:

$$Q_L = \frac{f_0}{\Delta f}. \quad (62)$$

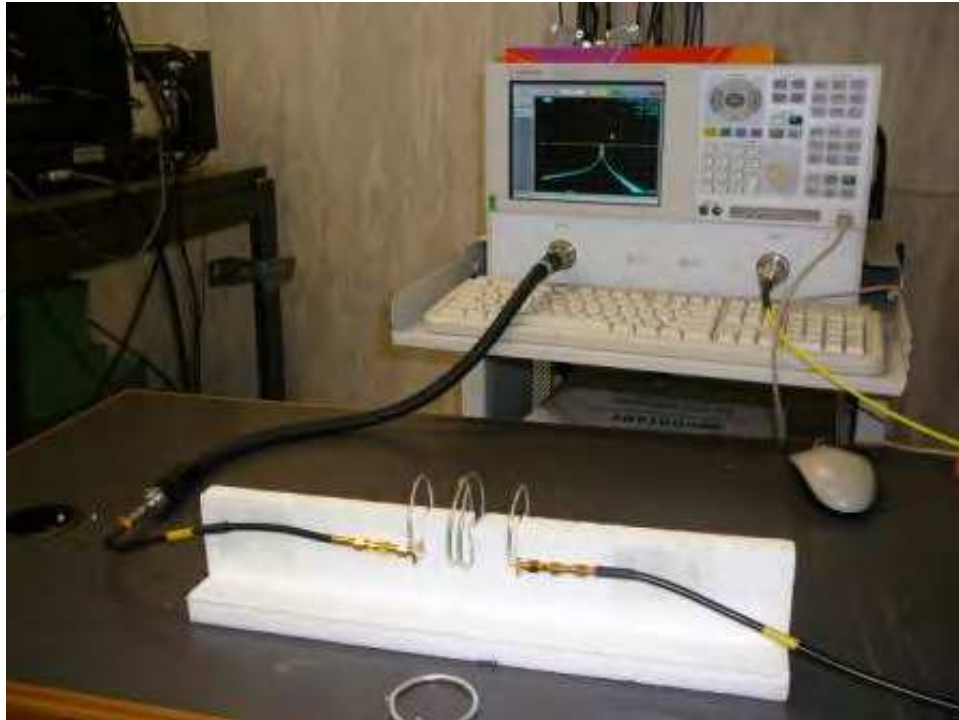


Fig. 31. Measurement setup with inductive loops and the resonator at the center.

Provided that a measure of the values of κ_1 and κ_2 has been performed, the unloaded quality factor is obtained as follows:

$$Q_0 = Q_L(1 + \kappa_1 + \kappa_2). \quad (63)$$

In particular, when the resonator is weakly coupled to the input and output loops, a simpler correction can be applied to the measured loaded Q_L factor as follows:

$$Q_0 = \frac{Q_L}{1 - |S_{21}|^2}. \quad (64)$$

This correction is widely used in practical cases.

5.2 Measurement set-up

In order to measure the resonant frequency and the Q factor of the resonators, two different setups can be adopted which depend on the chosen measurement type. The main instrument needed is a Vector Network Analyzer (VNA) and a single or a couple of coupling probes. In case of magnetically coupled resonators, circular inductive loops (balanced input) are used; a picture showing the measuring setup is given in Fig. 31.

There are some precautions that have to be followed: the first is to avoid conductive or magnetic materials close to the resonator because they can alter the magnetic field distribution and lead to unaccurate measurement. A second precaution is to test whether is necessary to add a 1:1 balun, between the balanced loop and the coaxial probe, in order to avoid unwanted current distributions on the measuring cables.

The distances between the loops and the resonator have to be adjusted in order to have the smallest coupling which still provide accurate measurements and, usually, an averaged measurement is employed.

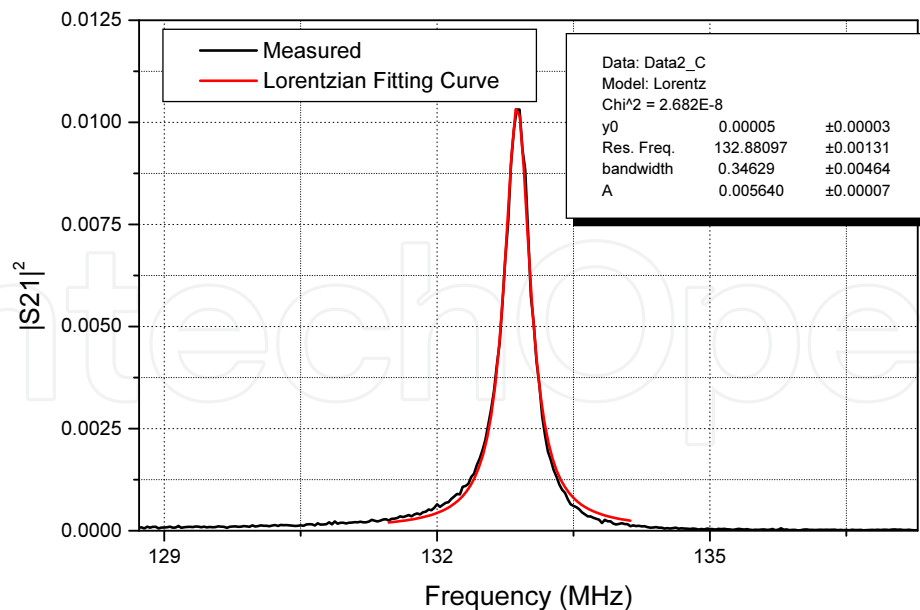


Fig. 32. Lorentzian fitting of the power transmission coefficient.

Once the measurement has been performed, it is possible to obtain the resonant frequency and the loaded Q factor either directly on the VNA, or by performing a fitting of the power transmission coefficient with a suitable peak fitting function.

As an example, a Lorentz function (see Fig. 32), whose expression is given by the following formula, may be used:

$$y(f) = y_0 + \frac{2A}{\pi} \frac{w}{4(f - f_0)^2 + w^2} \quad (65)$$

where y_0 is a constant value A is an amplitude scaling value, w the half power bandwidth and f_0 the resonant frequency. By following this procedure, a quite accurate measurement of resonant frequency and quality factor can be accomplished.

6. Conclusions

We have considered the problem of *resonant wireless electromagnetic energy transfer* over a medium range (from a fraction to a few times the resonator dimension). It has been shown that, by using network theory, considerable progress is feasible and a very high efficiency is attainable for the resonant inductive link. In particular, if the distance between the resonators is kept constant, by a suitable design of the matching networks, an optimal connection can be established for a given quality factor and coupling of the resonators.

For the case of resonators operating over variable distances, a new power oscillator, based on a Royer topology, has been proposed and an entire system has been studied and experimentally verified. A methodology for the analysis of more complex structures, including multiple transmitting and receiving resonators, has also been illustrated and Q measurement has been discussed.

As a final remark we note that resonant wireless power transfer is a new methodology, still under rapid development (see e.g. the notes of the workshop organized by Chen & Russer (2011)), which can be of considerable help in many practical problems: from electrical vehicle

charging Imura et al. (2009), to implanted device in the human body Zhang et al. (2009), to immortal sensors Watfa et al. (2010), to battery free operated devices.

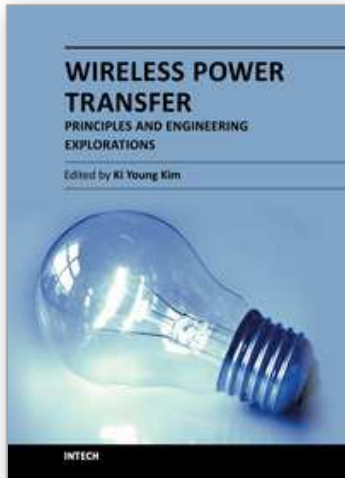
7. References

- R. E. Collin, (1960). *Field theory of guided waves*, Mc-Graw-Hill Book Co., New York.
- T. Rozzi and M. Mongiardo, (1997). *Open Electromagnetic Waveguides*, IEE, London.
- L.B. Felsen and M. Mongiardo and P. Russer, (2009). *Electromagnetic Field Computation by Network Methods*, Springer, Berlin.
- M. Mongiardo, C. Tomassoni, P. Russer, R. Sorrentino (2009), Rigorous Computer-Aided Design of Spherical Dielectric Resonators for Wireless Non-Radiative Energy Transfer, *MTT-S International Microwave Symposium*, Boston, USA.
- A. Kurs, A. Karalis, R. Moffatt, J. D. Joannopoulos, P. Fisher, and M. Soljacic (2007), Wireless Power Transfer via Strongly Coupled Magnetic Resonances, *Science*, 317, pp. 83-86.
- A. Karalis, J.D. Joannopoulos, M. Soljacic (2008), Efficient wireless non-radiative mid-range energy transfer," *Annals of Physics*, Elsevier, 323, pp. 24-48.
- B.L. Cannon, J.F. Hoburg, D.D. Stancil, S.C. Goldstein (2009), Magnetic Resonant Coupling As a Potential Means for Wireless Power Transfer to Multiple Small Receivers, *IEEE Transactions on Power Electronics*, vol.24, no.7, pp.1819-1825.
- M. Dionigi, M. Mongiardo, R. Sorrentino and C. Tomassoni (2009), Networks Methods for Wireless Resonant Energy Links (WREL) Computations, *ICEAA*, Turin, Italy.
- M. Dionigi, M. Mongiardo, (2010), CAD of Wireless Resonant Energy Links (WREL) Realized by Coils, *MTT-S International Microwave Symposium*, Anaheim, CA, USA, pp. 1760 - 1763.
- M. Dionigi, P. Mezzanotte, M. Mongiardo (2010), Computational Modeling of RF Wireless Resonant Energy Links (WREL) Coils-based Systems, *ACES Conference*, Tampere, Finland.
- M. Dionigi, M. Mongiardo, (2011), CAD of Efficient Wireless Power Transmission Systems, *MTT-S International Microwave Symposium*, Baltimore, MD, USA.
- M. Dionigi, M. Mongiardo, (2011), Efficiency Investigations for Wireless Resonant Energy Links Realized with Resonant Inductive Coils, *GEMIC, German Microwave Conference*.
- K. Finkenzeller (2003), *RFID handbook: fundamentals and applications in contactless smart cards*. Library of congress cataloging in publication data.
- W. Grover (2004), *Inductance Calculations*, Dover.
- V. Rizzoli, A. Costanzo, F. Matri and C. Cecchetti (1994), Harmonic-balance optimization of microwave oscillators for electrical performance, steady-state stability, and near-carrier phase noise, *IEEE MTT-S Int. Microwave Symp. Digest*, San Diego, pp. 1401-1404.
- D. Kajfez and P. Guillon, (1998). *Dielectric Resonators*, Noble Publishing Corporation, Atlanta.
- Z. Chen, P. Russer (organizers), (2011), WFA Workshop on Wireless Power Transmission, *MTT-S International Microwave Symposium*, Baltimore, MD, USA.
- T. Imura, H. Okabe, Y. Hori (2009), Basic Experimental Study on Helical Antennas of Wireless Power Transfer for Electric Vehicles by using Magnetic Resonant Couplings, *Vehicle Power and Propulsion Conference, IEEE*, Pages 936-940.
- F. Zhang, X. Liu, S.A. Hackworth, R.J. Scwabassi, M. Sun (2009), In vitro and in vivo studies on wireless powering of medical sensors and implantable devices, *Life Science Systems and Applications Workshop, IEEE/NIH*, Bethesda, MD, pp. 84 - 87.

M.K. Watfa, H. Al-Hassanieh, S. Salmen (2008), The Road to Immortal Sensor Nodes, *ISSNIP, International Conference on Intelligent Sensors, Sensor Networks and Information Processing*, Sydney, NSW, pp. 523 - 528.

IntechOpen

IntechOpen



Wireless Power Transfer - Principles and Engineering Explorations

Edited by Dr. Ki Young Kim

ISBN 978-953-307-874-8

Hard cover, 272 pages

Publisher InTech

Published online 25, January, 2012

Published in print edition January, 2012

The title of this book, *Wireless Power Transfer: Principles and Engineering Explorations*, encompasses theory and engineering technology, which are of interest for diverse classes of wireless power transfer. This book is a collection of contemporary research and developments in the area of wireless power transfer technology. It consists of 13 chapters that focus on interesting topics of wireless power links, and several system issues in which analytical methodologies, numerical simulation techniques, measurement techniques and methods, and applicable examples are investigated.

How to reference

In order to correctly reference this scholarly work, feel free to copy and paste the following:

Marco Dionigi, Alessandra Costanzo and Mauro Mongiardo (2012). Network Methods for Analysis and Design of Resonant Wireless Power Transfer Systems, *Wireless Power Transfer - Principles and Engineering Explorations*, Dr. Ki Young Kim (Ed.), ISBN: 978-953-307-874-8, InTech, Available from: <http://www.intechopen.com/books/wireless-power-transfer-principles-and-engineering-explorations/network-methods-for-the-analysis-and-design-of-wireless-power-transfer-systems>

INTECH

open science | open minds

InTech Europe

University Campus STeP Ri
Slavka Krautzeka 83/A
51000 Rijeka, Croatia
Phone: +385 (51) 770 447
Fax: +385 (51) 686 166
www.intechopen.com

InTech China

Unit 405, Office Block, Hotel Equatorial Shanghai
No.65, Yan An Road (West), Shanghai, 200040, China
中国上海市延安西路65号上海国际贵都大饭店办公楼405单元
Phone: +86-21-62489820
Fax: +86-21-62489821

© 2012 The Author(s). Licensee IntechOpen. This is an open access article distributed under the terms of the [Creative Commons Attribution 3.0 License](#), which permits unrestricted use, distribution, and reproduction in any medium, provided the original work is properly cited.

IntechOpen

IntechOpen